Does Humidity's Seasonal Cycle Affect the Annual-Mean Tropical Precipitation Response to Sulfate Aerosol Forcing?

TIMOTHY M. MERLIS

McGill University, Montreal, Quebec, Canada

(Manuscript received 1 June 2015, in final form 22 November 2015)

ABSTRACT

Sulfate aerosol radiative forcing alters the distribution of tropical precipitation in climate model simulations. The annual-mean tropical precipitation change is typically described as arising from an annual-mean change in the mean atmospheric circulation. However, the seasonality of the climatology of tropical humidity may modulate the annual-mean precipitation response. Here, the role of seasonality of tropical humidity is assessed using reanalysis and idealized atmospheric general circulation model (GCM) simulations perturbed by sulfate aerosol radiative forcing. When coupled to an aquaplanet slab ocean with low thermal inertia, the seasonal cycle in GCM simulations of the "continental" regime is large and the annual-mean precipitation change depends on both the seasonally varying perturbation mean meridional circulation and the seasonally varying climatological specific humidity. When coupled to an aquaplanet slab ocean with a higher thermal inertia, the seasonal cycle in GCM simulations of the "oceanic" regime is smaller and the annual-mean precipitation change can be approximated by considering the perturbation convergence of the water vapor flux of the annual-mean perturbation mean meridional circulation and the annual-mean climatological specific humidity. The results of the aquaplanet simulations taken together with the magnitude of the seasonality of humidity in an atmospheric reanalysis suggest that the simplest forms of energetic arguments for the tropical precipitation response to perturbations in the atmospheric energy budget, which neglect an explicit role for the seasonality of the radiative forcing and the climatological specific humidity, are not quantitatively accurate for Earth's tropical land regions.

1. Introduction

Consideration of atmospheric energetics has been a useful framework for understanding the response of tropical circulations and the concomitant precipitation changes to radiative forcing (Chou and Neelin 2004; Yoshimori and Broccoli 2008; Merlis 2015; Feldl and Bordoni 2016). The canonical example of this approach is the interpretation of shifts in the intertropical convergence zone (ITCZ) from hemispheric asymmetry in the top-of-atmosphere (TOA) radiative imbalance or surface fluxes. An asymmetry in forcing provokes interhemispheric energy transport by energetically direct circulations that converge water vapor into the hemisphere with the TOA energy surplus (Kang et al. 2008, 2009; Yoshimori and Broccoli 2008; Kang and Held 2012; Frierson and Hwang 2012; Donohoe et al. 2013; Bischoff and Schneider 2014). These results have been encapsulated in diffusive closures for the anomalous interhemispheric energy transport (Kang et al. 2009; Frierson and Hwang 2012; Bischoff and Schneider 2014). In practice, these approaches consider the response of annual-mean precipitation to annual-mean circulation changes that result from annual-mean changes in the spatial pattern of the TOA radiative forcing, radiative feedbacks, or surface fluxes (Frierson and Hwang 2012; Hwang et al. 2013; Bischoff and Schneider 2014).

Here, the role of the seasonal cycle of the climatological humidity on the annual-mean precipitation response to the radiative forcing of anthropogenic sulfate aerosols is assessed in an idealized atmospheric general circulation model (GCM). Anthropogenic sulfate aerosols are a forcing agent of particular interest in this context because their radiative forcing has seasonal variation that arises both from seasonality in their concentration (which can arise from precursor emissions

Corresponding author address: Timothy M. Merlis, Dept. of Atmospheric and Oceanic Sciences, McGill University, 805 Sherbrooke Street West, Montreal QC H3A 2K6, Canada.
E-mail: timothy.merlis@mcgill.ca

DOI: 10.1175/JCLI-D-15-0388.1

© 2016 American Meteorological Society

Unauthenticated | Downloaded 04/11/21 05:20 AM UTC

and the physical climate's influence on aerosol growth and aerosol sinks) and from the seasonality of insolation. Furthermore, anthropogenic sulfate aerosols have been invoked as critical to observed changes in the Indian monsoon (Bollasina et al. 2011) and zonal-mean tropical precipitation shifts (Hwang et al. 2013).

In what follows, idealized aquaplanet GCM simulations with either low or moderate homogeneous surface thermal inertias are subjected to sulfate aerosol radiative forcing to illustrate the potential importance of the seasonal cycle of the climatological humidity for annual-mean precipitation changes. The idealized simulations reveal a rectification mechanism in which seasonally varying perturbation winds and seasonally varying climatological humidity can produce an annual-mean tropical precipitation change: the annual-mean water vapor flux by the seasonally varying fields is larger than the water vapor flux of the annual-mean fields (section 3b). This mechanism implies that annual-mean precipitation changes do not directly follow annual-mean circulation changes. The geographic importance of the rectification mechanism in Earth's climate is then qualitatively assessed in a reanalysis estimate of the seasonal cycle of humidity (section 4).

2. Idealized GCM

The GCM described in Merlis et al. (2013a), which has comprehensive radiation transfer (from the Geophysical Fluid Dynamics Laboratory's AM2; Anderson et al. 2004) with prescribed clouds and an active hydrological cycle with an idealized quasi-equilibrium convection scheme (Frierson 2007), is used here. The prescribed cloud distribution has meridionally varying low clouds to produce an earthlike equator-to-pole temperature gradient and no high clouds [with the same parameters as in Merlis et al. (2013a)]. This GCM configuration allows for the water vapor feedback and suppresses cloud feedbacks. Suppressing cloud feedbacks will influence the magnitude of circulation changes, but these cloud-related circulation changes depend on model formulation (Voigt et al. 2014; Feldl and Bordoni 2016; Voigt and Shaw 2015). The idealized GCM, then, focuses attention on changes that depend on robust aspects of climate simulations.

I present the results of aquaplanet simulations with 5- and 20-m slab ocean depth. The simulations with low surface thermal inertia will be referred to as continental and the higher thermal inertia simulations will be referred to as oceanic in what follows. While a 20-m slab ocean depth is shallow compared to the mixed layer depth of many regions of the ocean, it is sufficiently deep that the results are distinct from the continental regime. In all cases, there is an infinite water supply at the surface for evaporation. The use of the aquaplanet lower boundary condition is an idealization that removes the quantitatively important, but complicating, influence of spatial variations in the surface energy storage that arise from land–sea heat capacity contrasts. The insolation is that of a circular orbit (0 eccentricity) with orbital obliquity of 23.5°. Thus, the boundary conditions and forcing are hemispherically symmetric in the time mean, except for the prescribed aerosol concentration. The simulations are performed with T85 spectral resolution and 30 vertical levels, although the results are similar with T42 resolution. All other parameters follow those of Merlis et al. (2013a). Simulations are integrated for 30 yr and averages over the last 20 yr are presented.

The control simulations have prescribed preindustrial sulfate aerosol concentration with all other aerosol concentrations are zero. Following Yoshimori and Broccoli (2008), the perturbation simulations have a prescribed sulfate aerosol concentration of 2.2 times the anthropogenic perturbation (defined as the difference between 2000 and 1860) from a chemical transport model (Horowitz et al. 2003). The increased amplitude of the forcing has the virtue of generating a larger forced response and the central results presented here are unchanged in simulations with a 1 times perturbation sulfate aerosol concentration. Radiative forcing is estimated using fixed-SST simulations (Hansen et al. 2005; Yoshimori and Broccoli 2008). The forcing has largest magnitude in the Northern Hemisphere extratropics and is weak in the Southern Hemisphere (Figs. 1b and 2b). Seasonally, it is largest in Northern Hemisphere summer (Figs. 1b and 2b). Because only low clouds are prescribed, the magnitude of the radiative forcing in the idealized GCM is greater than comprehensive AM2.1 simulations by approximately a factor of 2 in the global and annual mean [$-4.4\,\mathrm{W\,m^{-2}}$ for 5-m depth and $-4.7\,\mathrm{W\,m^{-2}}$ for 20-m slab ocean depth compared to $-2.0\,\mathrm{W\,m^{-2}}$ in the simulations of Yoshimori and Broccoli (2008)].

Additional simulations with zonally symmetrized aerosol concentrations have similar zonal-mean tropical precipitation responses. This results from the zonally symmetric aquaplanet boundary condition (Kang et al. 2014), so the meridional and temporal variations in the forcing are the aspects critical to the results presented here. In section 3c, the importance of seasonal variations in the forcing is assessed by comparing to a simulation with a time-independent energy sink in the slab ocean that has the meridional structure and amplitude of the annual- and zonal-mean sulfate aerosol radiative forcing (Fig. 1b).

Unauthenticated | Downloaded 04/11/21 05:20 AM UTC

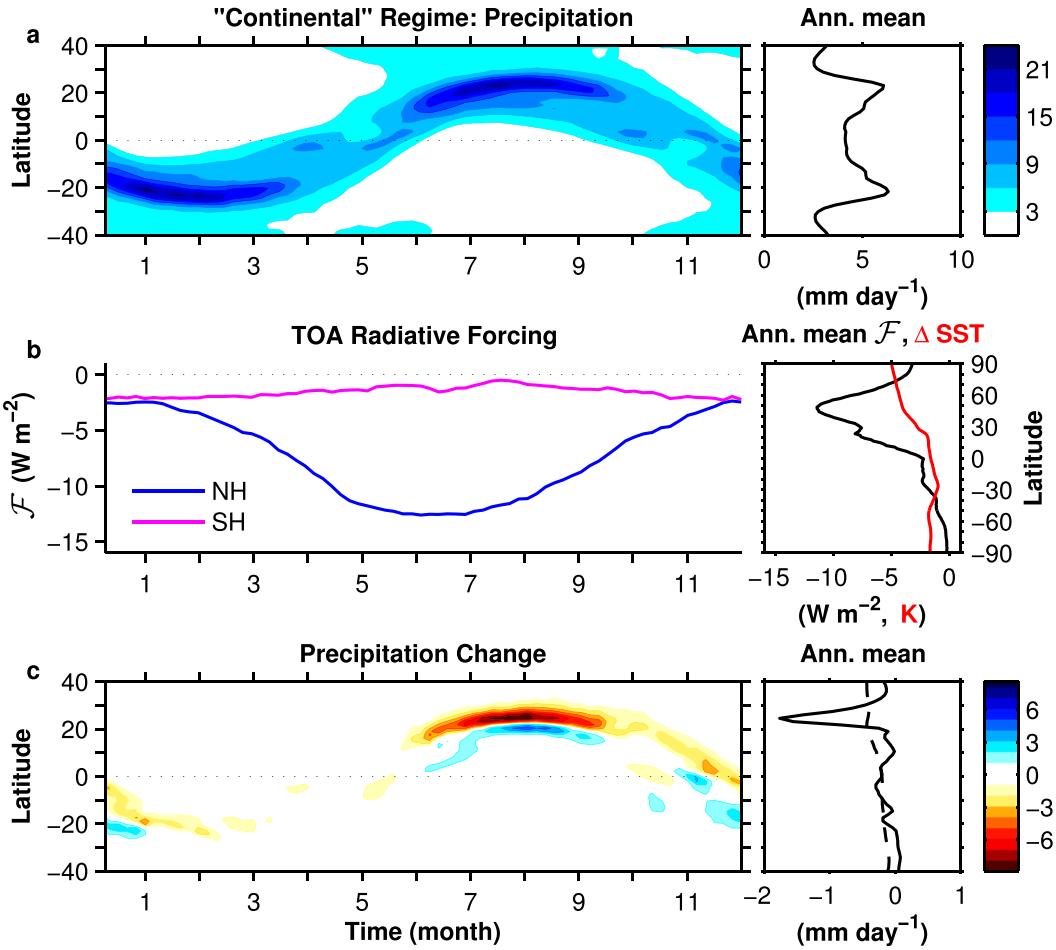

FIG. 1. (a) Seasonal cycle of zonal-mean precipitation (color contouring with 3 mm day^{-1} interval) with annual- and zonal-mean precipitation for the control continental regime simulation with slab ocean depth of 5 m. (b) Seasonal cycle of hemisphere-mean sulfate aerosol radiative forcing in Northern (blue) and Southern (magenta) Hemisphere with annual- and zonal-mean radiative forcing (black) and surface temperature change (red). (c) Seasonal cycle of response of zonal-mean precipitation (color contouring with 1 mm day^{-1} interval) with annual- and zonal-mean response of precipitation (solid line) and evaporation (dashed line) to sulfate aerosol radiative forcing.

3. Precipitation response to sulfate aerosols

a. Simulation results

Figure 1a shows the seasonal cycle of the climatological zonal-mean precipitation and its annual mean in the continental simulations with low surface thermal inertia and the control preindustrial sulfate aerosol concentration. The ITCZ extends seasonally into the subtropics (as in similarly configured simulations; Bordoni and Schneider 2008; Merlis et al. 2013a; Donohoe et al. 2014), with a maximum latitude of ~25° following each hemisphere's solstice. The annual-mean precipitation has two off-equatorial maxima that correspond to the seasonal excursions of the ITCZ associated with the strong cross-equatorial or ''monsoonal'' Hadley circulation.

The control oceanic simulation with higher surface thermal inertia has weaker seasonal off-equatorial ITCZ excursions, reaching a maximum latitude of ~12° following the solstices, and the annual-mean precipitation has a well-defined equatorial maximum (Fig. 2a). For both the oceanic and continental control simulations, the deviation from symmetry between the hemispheres arises from limited time sampling and the nonzero preindustrial sulfate aerosol concentration.

In the continental regime, the tropical precipitation response to sulfate aerosol radiative forcing features decreases in the precipitation rate in the convergence zone and increases to its south over the seasonal cycle (Fig. 1c). The precipitation response is larger in Northern Hemisphere summer and fall compared to the Southern Hemisphere summer and fall, and this

Unauthenticated | Downloaded 04/11/21 05:20 AM UTC

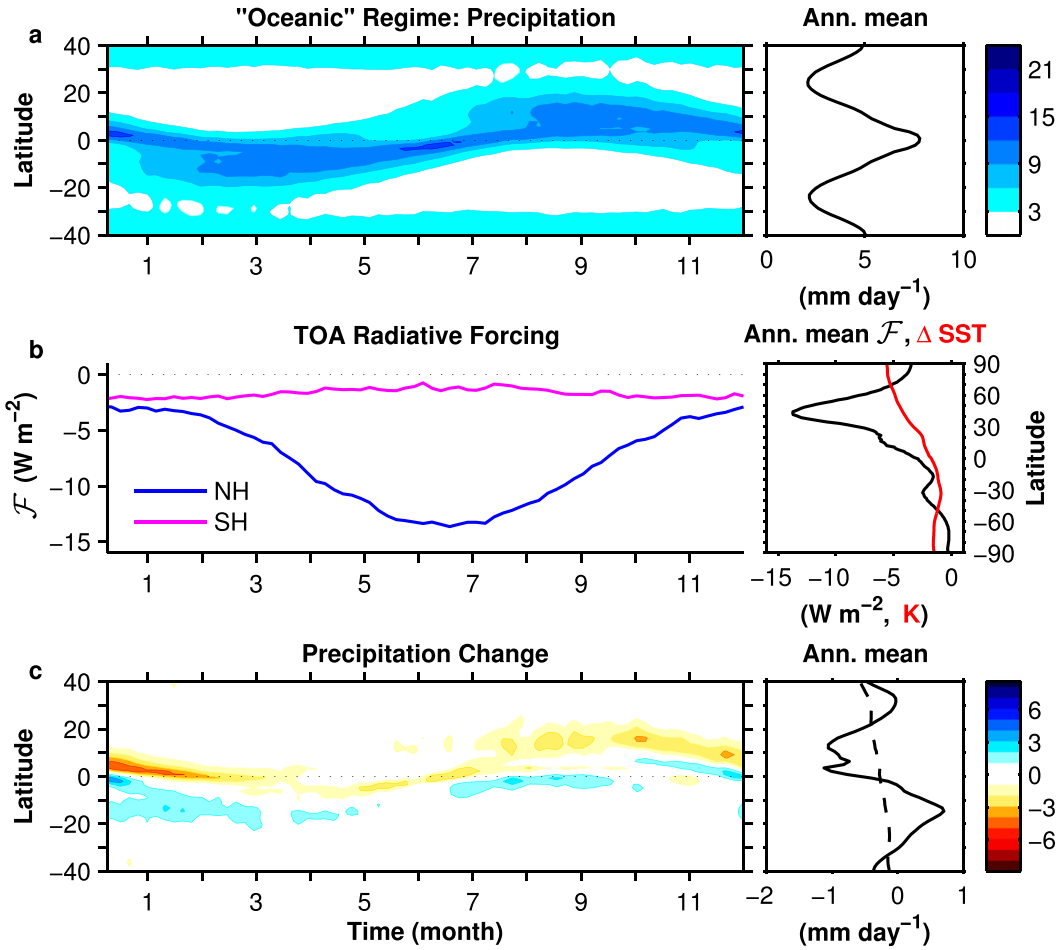

FIG. 2. As in Fig. 1, but for the oceanic regime with slab ocean depth of 20 m.

seasonality follows that of the radiating forcing (Fig. 1b) with an ~1-month phase lag. The annual-mean precipitation change is generally a decrease in the tropics, with a sharp decrease of ~1.8 mm day^{-1} that is confined to the northern edge (~25°) of the seasonal ITCZ. Away from this region, the magnitude of the annual-mean precipitation decrease is similar to the evaporation decrease (Fig. 1c). As expected from a reduction of absorbed solar radiation at the surface, evaporation decreases under sulfate aerosol radiative forcing. It is clear from the seasonal cycle of the precipitation change that the large annual-mean decrease near 25°N arises from the convergence zone's decrease in precipitation and southward shift in Northern Hemisphere summer. South of this (near 15°N) there are seasonally canceling changes as the southward shift in Northern Hemisphere summer increases precipitation, while there are precipitation decreases in the convergence zone in the transitions to and from the off-equatorial convergence zone extremum in the Northern Hemisphere spring and the Northern Hemisphere fall. The resulting annual-mean change in precipitation near 15°N is weak. Therefore, the annual-mean change is not simply a southward shift where the decrease in precipitation near 25°N is accompanied by an increase in precipitation to the south of this region. There are, however, regions of modest net precipitation (precipitation minus evaporation) increases adjacent to the strong decrease near 25°N.

The sulfate aerosol-forced precipitation change in the oceanic regime is a southward shift in the convergence zone that follows its seasonal off-equatorial excursions (Fig. 2). As in the continental simulations, the weakest change is in Northern Hemisphere spring, prior to the peak radiative forcing. However, the precipitation change in the oceanic regime has weaker seasonality, consistent with more of the radiative forcing being stored in the surface and affecting the surface fluxes, circulation, and precipitation in subsequent seasons. The annual-mean precipitation change has a dipole near the equator: a ~1 mm day^{-1} decrease in precipitation north of the equator and a ~0.7 mm day^{-1} increase precipitation

Unauthenticated | Downloaded 04/11/21 05:20 AM UTC

south of the equator (Fig. 2c). This southward shift of annual-mean tropical precipitation is broadly similar to others that have been described in comprehensive GCM simulations perturbed by sulfate aerosol radiative forcing [e.g., the simulation in Yoshimori and Broccoli (2008), which has hemispherically asymmetric tropical P and $P - E$ changes of $\sim$1 mm day^{-1} in the tropics].

b. Water vapor budget decomposition

The equilibrium annual-mean (indicated by square brackets) atmospheric water vapor budget relates precipitation minus evaporation $P - E$ (net precipitation) to the mass-weighted vertical integral (indicated by curly brackets) of the convergence of the water vapor flux $\mathbf{u}q$:

$$[P - E] = -\int_0^{p_s} \nabla \cdot [\mathbf{u}q]\frac{dp}{g} = -\nabla \cdot \{[\mathbf{u}q]\}, \qquad (1)$$

with horizontal wind vector $\mathbf{u}$, specific humidity q, and other symbols have their standard meaning. For climate changes, the monthly mean (indicated by an overbar) perturbation water vapor flux can be decomposed into dynamic and thermodynamic components (e.g., Chou and Neelin 2004; Held and Soden 2006; Merlis et al. 2013c):

$$\delta\overline{\mathbf{u}q} = \underbrace{\delta\overline{\mathbf{u}}\,\overline{q}}_{\text{dynamic}} + \underbrace{\overline{\mathbf{u}}.\overline{\mathscr{H}}\,\delta\overline{q}_s}_{\text{thermodynamic}} + \cdots, \qquad (2)$$

with relative humidity $\mathscr{H}$ and saturation specific humidity q_s. The variables immediately preceded by δ are perturbed variables, others are control variables, and additional terms arising from changes in relative humidity, transient eddy fluxes, and higher-order terms are suppressed. These additional terms are summed to form the "residual" shown in Fig. 3. The use of the monthly mean is a typical choice that brackets off the water vapor flux associated with transient eddies from that of the seasonally varying time-mean circulation.

Here I consider a further decomposition of the annual-mean dynamic water vapor flux change $[\delta\overline{\mathbf{u}}\,\overline{q}]$ by partitioning it into the flux of annual-mean humidity $[q]$ by the annual-mean perturbation velocity $\delta[\mathbf{u}]$ (referred to as the annual-mean dynamic component in what follows) and the deviation thereof: $[\delta\overline{\mathbf{u}}\,\overline{q}] = \delta[\mathbf{u}][q] + [\delta(\overline{\mathbf{u}} - [\mathbf{u}])(\overline{q} - [q])]$. The deviation term depends on the seasonality of both the perturbation winds $\delta(\overline{\mathbf{u}} - [\mathbf{u}])$ and the climatological specific humidity—the departure of the monthly mean specific humidity $\overline{q}$ from the annual-mean specific humidity $[q]$. Therefore, this term tends to zero if either the perturbation to the mean circulation *or* the climatology of humidity has weak seasonality.

Figures 3a and 3c show a decomposition of the annual-mean perturbation water vapor budget into dynamic and thermodynamic components. The dynamic component of the change in water vapor flux is the largest term in both the continental and oceanic simulations, although the thermodynamic component is not negligible in the oceanic simulations. While the pattern of annual-mean surface temperature change is broadly similar between the continental and oceanic simulations (Figs. 1b and 2b), the thermodynamic component differs because of the differences in the climatological circulations.

The annual-mean dynamic component (from the convergence of $\delta[\mathbf{u}][q]$) is shown in cyan lines in Figs. 3a and 3c. In the oceanic regime, it is nearly indistinguishable from the full dynamic component $[\delta\overline{\mathbf{u}}\,\overline{q}]$, formed with the seasonally varying monthly means. In contrast, it underestimates the variations of the full dynamic component in the Northern Hemisphere subtropics of the continental simulations (between 10° and 30°N). The underestimation is about 30% in the region near 25°N where the reduction in (net) precipitation is maximum (Fig. 3c, Table 1).

To further assess the magnitude and origin of the discrepancy between the annual-mean dynamic component and the full dynamic component, the water vapor flux is expressed as $\nabla \cdot (\delta\overline{\mathbf{u}}\,\overline{q}) = \overline{q}\nabla \cdot (\delta\overline{\mathbf{u}}) + \delta\overline{\mathbf{u}} \cdot \nabla\overline{q}$. The advection term $\delta\overline{\mathbf{u}} \cdot \nabla\overline{q}$ is small compared to the convergence term $\overline{q}\nabla \cdot (\delta\overline{\mathbf{u}})$ in the simulations: $-\nabla \cdot (\delta\overline{\mathbf{u}}\,\overline{q}) \approx -\overline{q}\nabla \cdot (\delta\overline{\mathbf{u}})$. A rectification of the seasonal cycles of the climatological specific humidity $\overline{q}$ and the perturbation convergence of the monthly-mean horizontal wind $\nabla \cdot (\delta\overline{\mathbf{u}})$ will result in an annual-mean precipitation change if the seasonal cycles are correlated.[1] Time series of these components that contribute to the dynamic component of the water vapor flux are presented next.

Figures 3b and 3d show the seasonal cycle near-surface specific humidity $\overline{q}$, perturbation convergence of the near-surface horizontal wind $-\nabla \cdot (\delta\overline{\mathbf{u}})$, and their product $-\overline{q}\nabla \cdot (\delta\overline{\mathbf{u}})$ evaluated in the Northern Hemisphere region of large annual-mean precipitation decrease. The full vertical integral is well approximated by a near-surface average because of the small-scale height of water vapor. The seasonal cycle of the climatological near-surface specific humidity is maximum in summer and is in phase with seasonal cycle of the perturbation near-surface convergence (or, equivalently,

[1] The thermodynamic rectification mechanism described in Merlis et al. (2013c) is distinct: it results from seasonal correlations between the perturbation specific humidity $\delta\overline{q}$ and the climatological convergence of the horizontal wind $\nabla \cdot \overline{\mathbf{u}}$.

Unauthenticated | Downloaded 04/11/21 05:20 AM UTC

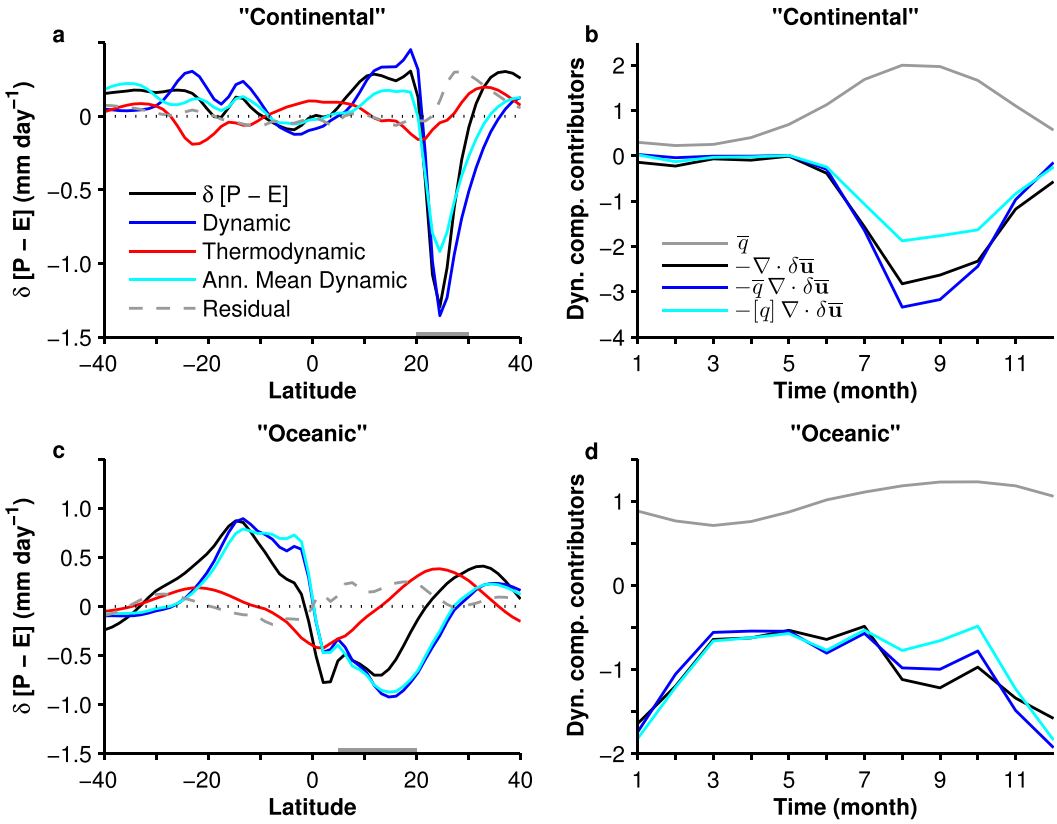

FIG. 3. Water vapor budget decomposition of change in annual- and zonal-mean net precipitation $\delta[P-E]$ for (a) continental and (c) oceanic simulations with dynamic, thermodynamic, and residual defined in section 3b. (b),(d) The importance of seasonality in the dynamical component of the change in water vapor flux is assessed by showing seasonal time series of the largest contributors $\overline{q}$ and $-\nabla\cdot(\delta\overline{\mathbf{u}})$, which are vertically integrated from the surface to $\sigma = p/p_s = 0.73$ in the region of large dynamic water vapor flux changes, as indicated by the gray line at the bottom of (a) and (c). Time series of $\overline{q}$, $-\nabla\cdot(\delta\overline{\mathbf{u}})$, and $-\overline{q}\nabla\cdot(\delta\overline{\mathbf{u}})$ are divided by the absolute value of their annual means. For the continental simulations in (b), these values are 6.7×10^{-3}, 3.0×10^{-7}, and $4.1\times10^{-9}\,\mathrm{s}^{-1}$, respectively. For the oceanic simulations in (d), they are 8.4×10^{-3}, 2.8×10^{-7}, and $2.8\times10^{-9}\,\mathrm{s}^{-1}$, respectively. The annual mean $-[q]\nabla\cdot(\delta\overline{\mathbf{u}})$ is normalized by the same value as the corresponding $-\overline{q}\nabla\cdot(\delta\overline{\mathbf{u}})$ to show the difference that seasonally varying humidity makes.

the perturbation vertical velocity at the top of the boundary layer). The role of the climatological seasonal cycle of humidity is illustrated by the cyan line: when the annual-mean humidity is used instead of the seasonally varying humidity, there is a substantial underestimate of the perturbation humidity convergence in the summer season and this reduces the annual-mean change in the continental regime (Fig. 3b, Table 1).

In contrast, the oceanic regime has relatively mild seasonality in both the climatological humidity and the perturbation convergence of the horizontal wind (Fig. 3d). Replacing the seasonally varying humidity by the annual mean does result in differences (an underestimate in Northern Hemisphere summer and an overestimate in Northern Hemisphere winter), although these largely cancel in the annual mean (Table 1). Therefore, the annual-mean rectification of the seasonal cycle is weak and the approximation of neglecting seasonality in humidity is adequate to determine annual-mean precipitation changes. The error of a few percent is similar to or smaller than the

TABLE 1. Changes in net precipitation, the dynamical component of the perturbation water vapor flux, and the annual-mean dynamic component of the perturbation water vapor flux (defined in section 3b; in mm day^{-1}) averaged over the regions indicated in Fig. 3.

Slab depth	Forcing	$\delta[P-E]$	Dynamic $[\delta\overline{\mathbf{u}}\,\overline{q}]$	Annual-mean dynamic $\delta[\mathbf{u}][q]$
20 m	AERO	−0.58	−0.75	−0.75
5 m	AERO	−0.82	−0.92	−0.66
5 m	QFLUX	−0.50	−0.60	−0.43

Unauthenticated | Downloaded 04/11/21 05:20 AM UTC

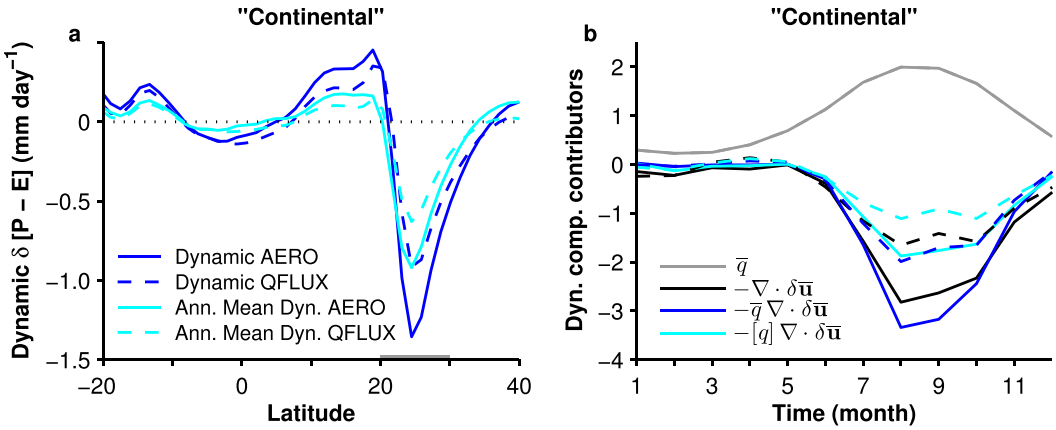

FIG. 4. (a) Dynamic component of the water vapor budget decomposition of change in annual- and zonal-mean net precipitation $\delta[P - E]$ for continental simulations with time-dependent aerosol radiative forcing AERO and time-independent surface energy sink QFLUX. (b) The importance of seasonality in the dynamical component of the change in water vapor flux is assessed by showing seasonal time series of the largest contributors $\overline{q}$ and $-\nabla\cdot(\delta\overline{\mathbf{u}})$, which are vertically integrated from the surface to $\sigma = p/p_s = 0.73$ in the region of large dynamic water vapor flux changes indicated by the gray line at the bottom of (a). Time series of $\overline{q}$, $-\nabla\cdot(\delta\overline{\mathbf{u}})$, and $-\overline{q}\nabla\cdot(\delta\overline{\mathbf{u}})$ in both AERO and QFLUX simulations are divided by the absolute value of the annual mean of the continental simulation with sulfate aerosol radiative forcing (values as in Fig. 3).

other approximations employed when the energetic framework has been applied to annual-mean tropical precipitation changes (e.g., holding the diffusivity used to parameterize energy transport fixed as the climate changes).

c. *Time-independent versus seasonal forcing in the continental regime*

The rectification mechanism described here relies on the combined effects of seasonally varying circulation changes and the seasonally varying climatology of humidity, so I present a simulation designed to assess the importance of the seasonally varying radiative forcing in producing the seasonally varying circulation changes. The annual- and zonal-mean radiative forcing (Fig. 1b) is applied as a time-independent sink in the slab ocean's surface energy evolution equation with the continental heat capacity of 5 m. The simulation with time-independent forcing has a weaker magnitude net precipitation change (~40%) and this is largely from a weaker magnitude dynamic component of the precipitation change (~35%) compared to the time-dependent aerosol forcing (Fig. 4a, Table 1). In both cases, the Northern Hemisphere summer change dominates the annual-mean circulation response, consistent with the monsoonal circulation approaching the angular momentum–conserving limit in which the atmospheric energy balance, rather than eddy momentum fluxes, controls its strength (Schneider 2006; Bordoni and Schneider 2008; Merlis et al. 2013b). Therefore, the simulation with time-independent forcing, with weaker forcing in Northern Hemisphere summer, has a weaker circulation change in both that season and in the annual mean relative to the simulation with time-dependent aerosol forcing (Fig. 4b). Since the seasonal dependence of the circulation change can result from either the seasonality in the radiative forcing or the seasonality in the regime of the momentum balance, the simulation with the time-independent forcing also has an ~30% discrepancy between the annual-mean dynamic component and the full dynamic component (Table 1).

An important role for seasonally varying forcing was also found in comprehensive GCM land-use change simulations analyzed in Kang et al. (2015): the Northern Hemisphere fall is less effective at provoking tropical precipitation changes than Northern Hemisphere spring because of a differences in the extent to which the forcing is balanced by local perturbations to the TOA budget rather than affecting meridional energy transport. Taken together, the results presented here and those in Kang et al. (2015) suggest that a full understanding of the tropical circulation response to extratropical forcing depends on 1) the seasonality of the forcing, 2) the accompanying local response of the TOA energy budget, and 3) circulation's seasonal momentum balance. With the knowledge of the seasonally varying circulation change, the analysis of the water vapor budget presented here demonstrates that one must additionally consider the seasonal cycle of the climatological humidity to determine the annual-mean precipitation change.

Unauthenticated | Downloaded 04/11/21 05:20 AM UTC

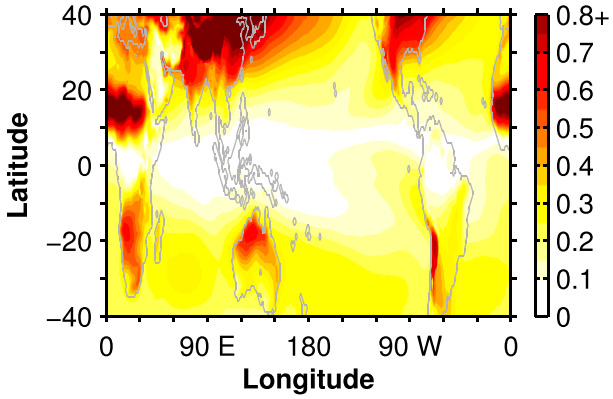

FIG. 5. Ratio of the first annual harmonic of monthly mean surface specific humidity to its annual mean in ERA-Interim for the climatology of 1981–2000.

4. Seasonality of the earth's humidity

The magnitude of the seasonality of the earth's near-surface humidity can be assessed in a reanalysis estimate to identify regions in which the rectification mechanism identified here is likely to be important for Earth's climate. Figure 5 shows the ratio of the first annual harmonic of surface specific humidity $\widehat{q}$ to the annual mean $[q]$ in the European Centre for Medium-Range Weather Forecasts interim reanalysis (ERA-Interim; Dee et al. 2011). The first annual harmonic is fit by minimizing the sum of squares for the climatology defined from 1981 to 2000. The amplitude of the seasonal cycle of humidity is weak over the ocean ($\sim$10% of the annual mean). In contrast, in nearly all subtropical continental regions, the seasonal cycle of humidity is large ($\gtrsim$40%) relative to the annual mean. The vertically integrated near-surface specific humidity (from surface to 750 hPa) has a similar magnitude and spatial pattern as the surface averaging convention shown in Fig. 5.

This measure of the amplitude of the seasonal cycle of humidity is relevant to determining the magnitude of annual-mean precipitation changes as follows. For regions with seasonal cycles that are well approximated by the first annual harmonic, $\overline{q}(t) = [q] + \widehat{q}\cos(\omega t + \phi_q)$ and $\delta\overline{\mathbf{u}}(t) = \delta[\mathbf{u}] + \widehat{\delta\mathbf{u}}\cos(\omega t + \phi_u)$ with $\omega = 2\pi\,\mathrm{yr}^{-1}$, the difference between the annual-mean dynamic component ($\propto\delta[\mathbf{u}][q]$) and the full dynamic component ($\propto[\delta\overline{\mathbf{u}}\,\overline{q}]$) will be maximum if the seasonal cycles are in phase $\phi_q = \phi_u$, as is approximately the case in the idealized GCM simulations (Fig. 3). The ratio of the annual-mean dynamic component to the full dynamic component is then

$$\frac{\delta[\mathbf{u}][q]}{[\delta\overline{\mathbf{u}}\,\overline{q}]} = \frac{\delta[\mathbf{u}][q]}{\delta[\mathbf{u}][q] + \frac{1}{2}\widehat{\delta\mathbf{u}}\widehat{q}} \approx 1 - \frac{\widehat{\delta\mathbf{u}}\widehat{q}}{2\delta[\mathbf{u}][q]}. \qquad (3)$$

Without explicitly evaluating seasonal circulation changes, a qualitative estimate of the magnitude of the importance of this annual-mean precipitation change mechanism is possible if magnitude of the seasonally varying near-surface wind changes relative to the annual-mean is comparable to that of the climatology of humidity $\widehat{\delta\mathbf{u}}/\delta[\mathbf{u}] \sim \widehat{q}/[q]$. This simple approximation that assumes regions with large seasonality in the climatology have large seasonality in their response to radiative forcing is appropriate in the idealized GCM simulations presented here (Fig. 3) and the analysis of comprehensive GCM simulations in Sobel and Camargo (2011) also shows substantial seasonality in tropical surface wind changes. Therefore, the underestimate of neglecting the deviations from the annual-mean dynamic component would have the same spatial pattern as Fig. 5 and would scale like its square.[2] Concretely, the annual-mean dynamic response in continental regions with $\widehat{q}/[q] \approx 0.6$ would underestimate the full dynamic response by about 20% with these assumptions about the circulation change's amplitude and phase. On one hand, discrepancies from neglecting the climatological seasonal cycle of humidity when estimating the annual-mean precipitation response are important in continental regions. On the other hand, the results suggest that the application of the energetic framework neglecting seasonality to the oceanic regions is well justified: errors from neglecting the seasonality of humidity are $\lesssim$10% according to this estimate.

5. Discussion and conclusions

By considering the role of seasonality in determining annual-mean tropical precipitation changes, I have identified a mechanism that produces annual-mean precipitation as the result of the water vapor flux of the seasonally varying perturbation tropical circulation and the seasonally varying climatological humidity. To date, the seasonal cycle of humidity has not been included in applications of the energetic framework to tropical precipitation shifts, which have considered the perturbation water vapor flux from the climatological annual-mean humidity and the perturbation annual-mean circulation. The magnitude of the mechanism identified here depends on the magnitude of the climatological seasonal cycle of specific humidity (Figs. 3 and 5).

[2] The first annual harmonic does not capture the seasonal cycle well in certain continental regions with wet-to-dry season humidity variations that exceed 100%, such as the African Sahel. In this case, the underestimate from neglecting the deviation from the annual-mean humidity is greater than suggested by (3).

Unauthenticated | Downloaded 04/11/21 05:20 AM UTC

Therefore, the answer to the question posed by the title, "Does humidity's seasonal cycle affect the annual-mean tropical precipitation response to sulfate aerosol forcing?" is yes in continental regions with strong seasonal cycles of humidity, and, for practical purposes, no in oceanic regions with weak seasonal cycles of humidity.

A key part of this rectification mechanism is the seasonal amplitude and phase of the perturbation circulation. The simulations here have a radiative forcing agent (sulfate aerosols) with strong seasonality that arises for the same reason as the climatological humidity seasonal cycle: Earth receives more sunlight in summer than winter. Replacing the time-dependent aerosol radiative forcing by its annual- and zonal-mean reduces the annual-mean precipitation change. However, even in the simulation with time-independent forcing, there is seasonality to the perturbation circulation, which can arise because of seasonality in the regime of the circulation's angular momentum balance, and the combined effects of the seasonality of the perturbation circulation and the climatological humidity will affect the annual-mean precipitation (Fig. 4).

The results described here have implications for the interpretation of past climate changes recorded in the proxy records of paleoclimate changes. First, the large-amplitude seasonal cycle of humidity in continental regions suggests knowledge of the seasonal cycle of climate perturbations would quantitatively alter the results of applications of the energetic framework to interpret the hydrological cycle changes recorded terrestrial paleoclimate proxies (cf. Schneider et al. 2014). Second, the simulation results in the continental regime have a substantial reduction in the (net) precipitation at the northern edge of the convergence zone that is not accompanied by a corresponding increase to the south (Figs. 1 and 3). Therefore, the expectation of a dipole pattern of compensating increases and decreases that underlies many discussions of convergence zone shifts may not be relevant to the seasonal extremum of convergence over continents.

Assessing the water vapor budget seasonally in monsoon regions (e.g., Clement et al. 2004; Li et al. 2015) readily captures the role of humidity's seasonality on precipitation changes. From this seasonal perspective, the challenge is to relate the seasonal circulation changes to the radiative forcing. In this case, one must consider the seasonality of the forcing and the concomitant differential surface energy storage between land and ocean (e.g., Chou and Neelin 2003; Merlis et al. 2013b).

Acknowledgments. I thank the European Centre for Medium-Range Weather Forecasts for providing the ERA-Interim data and Luke Davis for his assistance in preparing the reanalysis. This work benefitted from discussions at the May 2015 California Institute of Technology Keck Center workshop on Monsoons: Past, Present and Future and reviews from Aiko Voigt and an anonymous reviewer. The program code for the simulations, based on the Flexible Modeling System of the Geophysical Fluid Dynamics Laboratory, and the simulation results themselves are available upon request. I acknowledge the support of Compute Canada and Natural Science and Engineering Research Council Grant RGPIN-2014-05416.

REFERENCES

Anderson, J. L., and Coauthors, 2004: The new GFDL global atmosphere and land model AM2-LM2: Evaluation with prescribed SST simulations. *J. Climate*, **17**, 4641–4673, doi:10.1175/JCLI-3223.1.

Bischoff, T., and T. Schneider, 2014: Energetic constraints on the position of the intertropical convergence zone. *J. Climate*, **27**, 4937–4951, doi:10.1175/JCLI-D-13-00650.1.

Bollasina, M. A., Y. Ming, and V. Ramaswamy, 2011: Anthropogenic aerosols and the weakening of the South Asian summer monsoon. *Science*, **334**, 502–505, doi:10.1126/science.1204994.

Bordoni, S., and T. Schneider, 2008: Monsoons as eddy-mediated regime transitions of the tropical overturning circulation. *Nat. Geosci.*, **1**, 515–519, doi:10.1038/ngeo248.

Chou, C., and J. D. Neelin, 2003: Mechanisms limiting the northward extent of the northern summer monsoons over North America, Asia, and Africa. *J. Climate*, **16**, 406–425, doi:10.1175/1520-0442(2003)016<0406:MLTNEO>2.0.CO;2.

——, and ——, 2004: Mechanisms of global warming impacts on regional tropical precipitation. *J. Climate*, **17**, 2688–2701, doi:10.1175/1520-0442(2004)017<2688:MOGWIO>2.0.CO;2.

Clement, A. C., A. Hall, and A. J. Broccoli, 2004: The importance of precessional signals in the tropical climate. *Climate Dyn.*, **22**, 327–341, doi:10.1007/s00382-003-0375-8.

Dee, D. P., and Coauthors, 2011: The ERA-Interim reanalysis: Configuration and performance of the data assimilation system. *Quart. J. Roy. Meteor. Soc.*, **137**, 553–597, doi:10.1002/qj.828.

Donohoe, A., J. Marshall, D. Ferreira, and D. Mcgee, 2013: The relationship between ITCZ location and cross-equatorial atmospheric heat transport: From the seasonal cycle to the Last Glacial Maximum. *J. Climate*, **26**, 3597–3618, doi:10.1175/JCLI-D-12-00467.1.

——, D. M. W. Frierson, and D. S. Battisti, 2014: The effect of ocean mixed layer depth on climate in slab ocean aquaplanet experiments. *Climate Dyn.*, **43**, 1041–1055, doi:10.1007/s00382-013-1843-4.

Feldl, N., and S. Bordoni, 2016: Characterizing the Hadley circulation response through regional climate feedbacks. *J. Climate*, **29**, 613–622, doi:10.1175/JCLI-D-15-0424.1.

Frierson, D. M. W., 2007: The dynamics of idealized convection schemes and their effect on the zonally averaged tropical circulation. *J. Atmos. Sci.*, **64**, 1959–1976, doi:10.1175/JAS3935.1.

——, and Y.-T. Hwang, 2012: Extratropical influence on ITCZ shifts in slab ocean simulations of global warming. *J. Climate*, **25**, 720–733, doi:10.1175/JCLI-D-11-00116.1.

Unauthenticated | Downloaded 04/11/21 05:20 AM UTC

Hansen, J., and Coauthors, 2005: Efficacy of climate forcings. *J. Geophys. Res.*, **110**, D18104, doi:10.1029/2005JD005776.

Held, I. M., and B. J. Soden, 2006: Robust responses of the hydrological cycle to global warming. *J. Climate*, **19**, 5686–5699, doi:10.1175/JCLI3990.1.

Horowitz, L. W., and Coauthors, 2003: A global simulation of tropospheric ozone and related tracers: Description and evaluation of MOZART, version 2. *J. Geophys. Res.*, **108**, 4784, doi:10.1029/2002JD002853.

Hwang, Y.-T., D. M. W. Frierson, and S. M. Kang, 2013: Anthropogenic sulfate aerosol and the southward shift of tropical precipitation in the late 20th century. *Geophys. Res. Lett.*, **40**, 2845–2850, doi:10.1002/grl.50502.

Kang, S. M., and I. M. Held, 2012: Tropical precipitation, SSTs and the surface energy budget: A zonally symmetric perspective. *Climate Dyn.*, **38**, 1917–1924, doi:10.1007/s00382-011-1048-7.

——, ——, D. M. W. Frierson, and M. Zhao, 2008: The response of the ITCZ to extratropical thermal forcing: Idealized slab-ocean experiments with a GCM. *J. Climate*, **21**, 3521–3532, doi:10.1175/2007JCLI2146.1.

——, D. M. W. Frierson, and I. M. Held, 2009: The tropical response to extratropical thermal forcing in an idealized GCM: The importance of radiative feedbacks and convective parameterization. *J. Atmos. Sci.*, **66**, 2812–2827, doi:10.1175/2009JAS2924.1.

——, I. M. Held, and S.-P. Xie, 2014: Contrasting the tropical responses to zonally asymmetric extratropical and tropical thermal forcing. *Climate Dyn.*, **42**, 2033–2043, doi:10.1007/s00382-013-1863-0.

——, B.-M. Kim, D. M. W. Frierson, S.-J. Jeong, J. Seo, and Y. Chae, 2015: Seasonal dependence of the effect of Arctic greening on tropical precipitation. *J. Climate*, **28**, 6086–6095, doi:10.1175/JCLI-D-15-0079.1.

Li, X., M. Ting, C. Li, and N. Henderson, 2015: Mechanisms of Asian summer monsoon changes in response to anthropogenic forcing in CMIP5 models. *J. Climate*, **28**, 4107–4125, doi:10.1175/JCLI-D-14-00559.1.

Merlis, T. M., 2015: Direct weakening of tropical circulations from masked CO_2 radiative forcing. *Proc. Natl. Acad. Sci. USA*, **112**, 13 167–13 171, doi:10.1073/pnas.1508268112.

——, T. Schneider, S. Bordoni, and I. Eisenman, 2013a: Hadley circulation response to orbital precession. Part I: Aquaplanets. *J. Climate*, **26**, 740–753, doi:10.1175/JCLI-D-11-00716.1.

——, ——, ——, and ——, 2013b: Hadley circulation response to orbital precession. Part II: Subtropical continent. *J. Climate*, **26**, 754–771, doi:10.1175/JCLI-D-12-00149.1.

——, ——, ——, and ——, 2013c: The tropical precipitation response to orbital precession. *J. Climate*, **26**, 2010–2021, doi:10.1175/JCLI-D-12-00186.1.

Schneider, T., 2006: The general circulation of the atmosphere. *Annu. Rev. Earth Planet. Sci.*, **34**, 655–688, doi:10.1146/annurev.earth.34.031405.125144.

——, T. Bischoff, and G. H. Haug, 2014: Migrations and dynamics of the intertropical convergence zone. *Nature*, **513**, 45–53, doi:10.1038/nature13636.

Sobel, A. H., and S. J. Camargo, 2011: Projected future seasonal changes in tropical summer climate. *J. Climate*, **24**, 473–487, doi:10.1175/2010JCLI3748.1.

Voigt, A., and T. A. Shaw, 2015: Circulation response to warming shaped by radiative changes of clouds and water vapour. *Nat. Geosci.*, **8**, 102–106, doi:10.1038/ngeo2345.

——, S. Bony, J.-L. Dufresne, and B. Stevens, 2014: The radiative impact of clouds on the shift of the intertropical convergence zone. *Geophys. Res. Lett.*, **41**, 4308–4315, doi:10.1002/2014GL060354.

Yoshimori, M., and A. J. Broccoli, 2008: Equilibrium response of an atmosphere-mixed layer ocean model to different radiative forcing agents: Global and zonal mean response. *J. Climate*, **21**, 4399–4423, doi:10.1175/2008JCLI2172.1.

Unauthenticated | Downloaded 04/11/21 05:20 AM UTC